Module 4: Interferometry

Lecture 22: Three dimensional convection phenomenon

The Lecture Contains:

Previous Next

Convection in a Horizontal Differentially Heated Fluid Layer

Overview

An experimental study of Rayleigh-Benard convection in an intermediate aspect ratio box that is square in plan is reported. An intermediate range of Rayleigh numbers has been considered in the study. The fluid employed is air. A Mach-Zehnder interferometer is used to collect the line-of-sight projections of the temperature field in the form of interferometric fringes. Images have been recorded after a sufficient time has elapsed for the initial transients to have been eliminated. Interferograms have been collected from four to six view angles. These are used to obtain the three-dimensional temperature field inside the cavity by using tomography. The MART algorithm has been used for the inversion of the projection data. The convergence of the iterative inversion procedure was unambiguous and asymptotic. The reconstructed temperature field with a subset of the total data was found to be consistent with the remaining unused projections.

Result for two Rayleigh numbers, namely 1.39×10^4 and 4.02×10^4 have been reported. These were found to correspond to two distinct flow regimes. At these Rayleigh numbers, a well-defined steady state was not observed. At the lower Rayleigh number, the fringes away from the wall showed mild unsteadiness. At the higher Rayleigh number, the fringes were found to switch between two patterns. Result for the dominate mode alone have been presented for this problem. At a Rayleigh number of 1.39×10^4 , three-dimensional flow structures, whose influence is equivalent to longitudinal rolls have been observed. At a Rayleigh number of 4.02×10^4, cubic cells have been noted in the cavity. The associated flow pattern is inferred to be a plume rising from the heated plate. The local Nusselt number variation is seen to be consistent with the observed flow patterns.

Motivation

Rayleigh-Benard convection in horizontal fluid layers is a problem of fundamental as well as practical importance. The flow pattern associated with this configuration shows a sequence of transitions from steady laminar to unsteady flow and ultimately to turbulence. This configuration has been studied by analytical and computational techniques as well as by experiments to understand the physics involved in the transition phenomena. Although extensive work has been reported, many questions remain to be answered. Many of the global features observed by numerical solutions are supported by experimental observations. However, a closer comparison in terms of thermal field and convection patterns remains to be carried out. With renewed interest in understanding nonlinear systems and simultaneously the availability of powerful computers, there has been a revival of interest in Rayleigh-Benard convection. The experimental technique has also been strengthened by the availability of optical methods to visualize the flow phenomena and computers for data storage, processing, and analysis.

Interferometric study of Rayleigh-Benard convection for two Rayleigh numbers (1.39×10^4 and 4.02×10^4) is reported in the present work. The cavity is square in plan and aspect ratio employed leads to an intermediate aspect ratio box. The aspect ratio is defined as the ratio of the horizontal dimension to the height of the cavity. The fluid considered is air. Results have been presented for flow patterns that develop at long-time that are after the initial transients have been eliminated. Interferograms collected from several line-of-sight projections have been processed to reconstruct the complete three-dimensional temperature field. The multiplicative algebraic reconstruction technique in a modified form called AVMART has been used as the preferred tomographic algorithm (AVMART)

Previous Next

Rayleigh-Benard Convection

The present state-of-understanding of Rayleigh-Benard convection is discussed below. In the simplest form, the flow configuration is comprised of a horizontal fluid layer confined between a pair of parallel horizontal plates. The fluid is differentially heated by maintaining the lower surface at a higher temperature compared to the top. This situation produces a top-heavy arrangement that is unstable. The dimensionless quantity that characterized the buoyancy-driven flow is the Rayleigh number defined as

$$Ra = \frac{g\beta\,(T_{hot} - T_{cold})\,h^3}{\nu\alpha} \qquad (17)$$

When Ra is below a critical value, the gravitational potential is not sufficient to overcome the viscous forces within the fluid layer. For Rayleigh numbers above the critical value, a steady flow is established. Subsequently, flow undergoes a sequence of transitions, finally resulting in turbulence.

Transitions in Rayleigh-Benard convection depend on a Rayleigh number, a Prandtl number, and the cavity aspect ratio. Additionally, there is an effect of the geometric structure of the side walls being straight or curved [113]. The present discussion is restricted to a rectangular cavity. For a fluid layer with an infinite aspect ratio, the first transition, namely the onset of fluid motion, occurs at a Rayleigh number of 1708, irrespective of the Prandtl number. The associated flow pattern is in the form of hexagonal cells. The general effect of lowering the aspect ratio is to stabilize the flow due to the presence of the side walls and thus increase the critical Rayleigh number. All subsequent transitions are Prandtl number dependent. The present discussion is devoted to Prandtl numbers in the range 0.7-7, for which some general conclusions can be drawn.

Flow patterns in rectangular cavities can be divided into three main categories, depending on the aspect ratio. These are small $(\approx 2-10)$, intermediate , $(\approx 10-30)$, and large $(\approx 30-60)$ aspect ratio boxes. Transition and chaos in a small aspect ratio enclosure with water has been experimentally studied by Nasuno et al. Their data is in good agreement with the stability diagram of Busse and Clever. In a large aspect ratio enclosure, it has been shown that flow beyond the critical Rayleigh number is always time-dependent and non-periodic (see Ahlers and Behringer). In contrast, a large number of bifurcations have been recorded both experimentally as well as in numerical studies in small aspect ratio enclosures. Information regarding intermediate aspect ratio enclosures is sparse. The transition sequence appears to be via the formation of longitudinal rolls that are aligned with the shorter side, polygonal cells; roll-loss and displacement; and finally towards turbulence.

When the Rayleigh number is close to the critical value for the onset of convection, hexagonal convection cells have been observed both experimentally and in computation [113]. With a further increase in the Rayleigh number, stable two-dimensional longitudinal rolls have been observed. Krishnamurti [120] is one of the earliest authors to conduct an experimental study and observe roll patterns. Much later, Kessler [121] obtained steady rolls formation through a numerical simulation. With further increase in the Rayleigh number, the two-dimensional rolls were seen to bifurcate slowly to three-dimensional rolls, showing variation in shape along the roll axis. The three-dimensional rolls were found to be steady over a range of Rayleigh numbers. For further increase in the Rayleigh number, a loss-of-roll phenomena was observed. Kirchartz and Oertel [116] have shown for a box of small aspect ratio the transition from four rolls to three rolls and finally to two rolls. Simultaneously, three-dimensional rolls become unstable and a periodic motion of the roll system begins along its axis. The critical Rayleigh number for the onset of oscillatory rolls is shown to be in the range of a

Rayleigh number of 30000 for air (Pr = 0.71) [121]. This critical Rayleigh number increases with the increase of the Prandtl number. The frequency of oscillation is not a strong function of the Rayleigh number, but increases slowly with increase in the Rayleigh number. Kessler [121] has also observed the exchange of mass between different rolls. This is due to a periodic motion in the location of the vertically upward and downward flow.

Previous Next

Experimental Details

The apparatus used to steady convection in the horizontal layer of air is shown in Figure 4.46. The cavity employed was 512×512 in plan, the vertical depth being adjustable. Two different vertical depths were used in the present study to generate the two Rayleigh numbers. For the higher Rayleigh number of 1.39×10^4, the vertical depth was 20mm. for the higher Rayleigh number 1.39×10^4, the vertical depth was 20mm. for the higher Rayleigh number of 4.02×10^4, the vertical depth was increased to 26.8mm. The aspect ratio was thus maintained at 25 and 18.6 respectively. The lowering of the aspect ratio was seen to reduce the extent of unsteadiness in the convection pattern at the higher Rayleigh number. The fluid layer was confined by two aluminum plates of 5mm thickness above and below. The side walls comprised of two superposed layers of Perspex sheets, each 10mm thick. A small window in the side walls enabled the recording of interfergrams. The top wall was cooled and the bottom wall was heated by pumping water continuously from constant temperature baths. Special attention was given to ensure that isothermal conditions prevailed at the aluminum plated. To produce a Rayleigh number of 1.39×10^4, the top wall is cooled to a temperature of $13.4^{\circ}C$ to a temperature of $30.5^{\circ}C$, while the bottom wall is heated of for a vertical depth of 20 mm. for Ra=4.02×10^4, the temperature difference was increased to $21.7^{\circ}C$ by cooling the upper plate to $12.4^{\circ}C$ and heating the bottom plate to $33.5^{\circ}C$, the cavity height being 26.8 mm. the ambient temperatures was $21.7^{\circ}C$ in all the experiments. Both walls were maintained at their respective temperatures to within 0° for the complete duration of the experiment. The temperatures of the walls were continuously monitored using thermocouples connected to a 30-channel temperature recorder. The entire test cell was placed was mounted over a traversing mechanism capable of both translational and rotational motion. The traversing mechanism was padded with a rubber sheet, 30 mm thick, to damp external vibrations. The interferometer was itself mounted on four pneumatic legs. A variety of tests were carried out to ensure that the convection patterns in the fluid layer were insensitive to external disturbances such as floor vibration and the flowing water. It was thus established that air convection patterns reached steady state in three to four hours. The experiment was conducted beyond four hours to eliminate the initial transients and obtain a dynamic steady state.

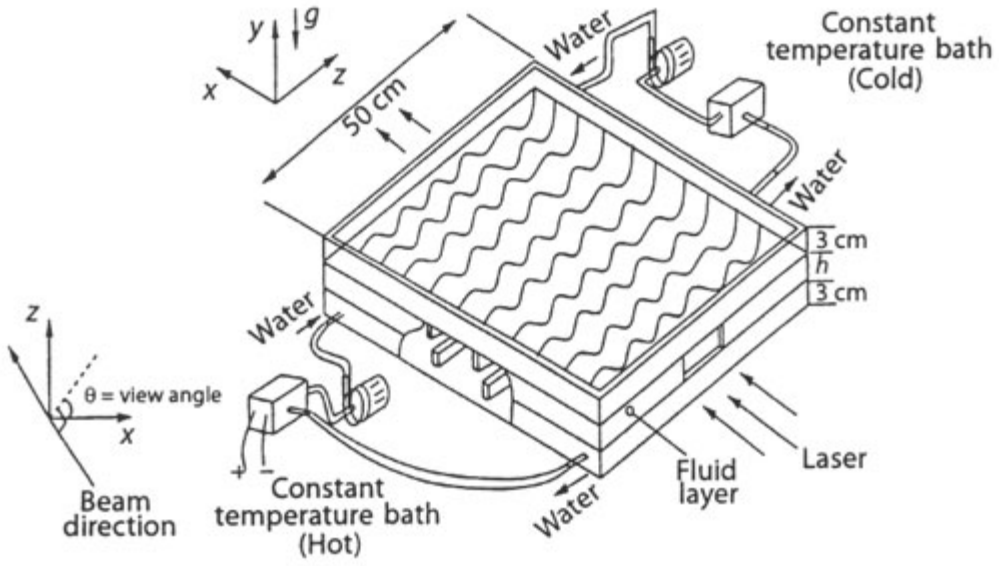

Figure 4.46: Schematic of the experimental appratus

Previous Next

Uncertainty and Measurement Errors

Errors in the experimental data are associated with misalignment of the apparatus with respect to the light beam, image processing operations including filtering, thinning and assigning temperature to fringes, error amplification during three-dimensional reconstruction, and the intrinsic uncertainly in the convection process itself. Errors related to refraction effects have been found to be quite small. All experiments were conducted several tomes to establish the repeatability of the fringe patterns. Time-dependent movement of fringes was not a source of uncertainly in the present work at a Rayleigh number of 1.39×10^4. However, at a Rayleigh number of 4.02×10^4, two sets of convection patterns were seen to be formed. Analysis has been carried out for the fringes patterns that formed for the most part of the experiment. The associated uncertainly in the local Nusselt number was found to be $\pm 20\%$ with 95% confidence. At both Rayleigh numbers, the plate-averaged Nusslet number was found to be in good agreement with published correlations and is discussed in Section Result and Discussion.The width-averaged temperature profile that represents energy balance across the cavity was also found to be unique and well-defined. Hence, the result obtained in the present work can be taken to be qualitatively meaningful.

Image Processing and Data Reduction

The three-dimensional reconstruction of the temperature field requires a noise-free set of projection data as input. Hence, prior to the calculation of the projection data in terms of the temperature, interferometric images have to be cleaned.

The projection data of the temperature field in the fluid layer is available at this stage in the form of temperatures at locations defined by the fringe geometry. To apply a tomographic algorithm, the projection data is required over a uniform grid. In the present study, two-dimensional quadratic Interpolation has been employed to transfer projection data from the fringe patterns to a uniform grid. The cavity height was discretized into 21 horizontal planes. The number of vertical columns at which interpolation was carried out for the 0° and 90° projections was 120. For the angular interpolations, the cavity width was effectively larger. However, the extreme ends of the cavity could not be due to reduction in the path length of the light beam trsversing the fluid layer. At these locations, there was a drastic reduction int he number of fringes and corresponding increase in the fringe spacing. Hence, for angular projections, only 160 vertical columns covering 60% of the cavity width were considered. The error introduced in the projection data dur to interpolation was found to be less than 0.01%.

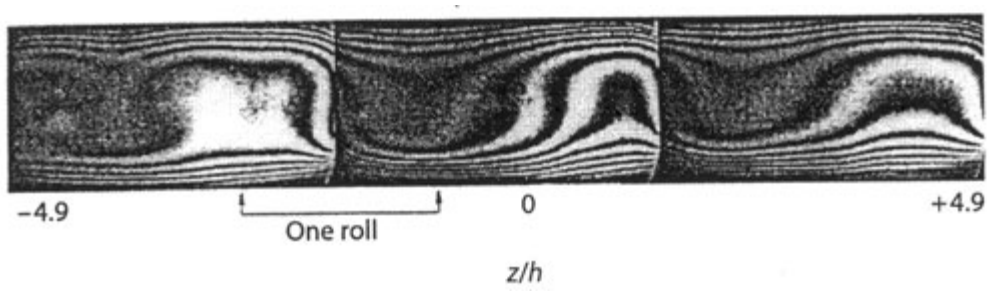

Figure 4.47: Original interferograms showing 5 full and 2 partial rolls at $Ra=1.39 \times 10^4$, 90° projection.

more...

Previous Next

Three-Dimensional Reconstruction Algorithm

The temperature data available on a Cartesian grid for each view angle represents the line integral of the temperature field in the fluid layer. Reconstruction of the three-dimensional temperature field form the projection data requires the use of tomographic algorithms. AVMART algorithm discussed in section 6.5 has been used in the present analysis.

A check on the correctness of the reconstructed field was carried out along the following lines. For a Rayleigh number of 1.39×10^4, six different set of projections were collected. Of these, four projections were used to reconstruct the three-dimensional temperature filed inside the cavity. The reconstructed field was used to compute the projections numerically at the two angles not included in the tomographic algorithm. These two projections (0° and 90°) were recorded. Besides this, for view angles of 30^0 and 60°, projections of the near central region of the cavity over a width of 6.2 cm were collected to serve as a cross-check for the reconstructed field.

The comparison between the numerically generated projections and the experimentally recorded interferograms not utilized in reconstruction is now presented. The Rayleigh number is 1.39×10^4, but similar checks were also carried out at $Ra=4.02 \times 10^4$. The cross-checks have been carried out at view angles of 30° and 120° in terms of isotherms, Figure 4.52. The close match between the two sets of data confirms the correctness of the reconstructed temperature field. A similar cross-check was carried out in terms of local Nusselt numbers at these projection angles and the comparison was found to be good.

Previous Next

Result and Discussion

Results have been presented for two Rayleigh numbers, namely 1.39×10^4 and 4.02×10^4. The flow structure and roll pattern, temperature filed over horizontal planes, and the wall Nusslet numbers have been reported. An earlier report of the present work at a Rayleigh number of 34800 with partial projection data at the view angles has been reported elsewhere [79]. Experiments were conducted at a fourth Rayleigh number if 51800 as well. The flow field at this Rayleigh number was found to be completely unsteady with no noticeable periodicity. Hence images even at neighboring positions were seen to be uncorrelated. Tomographic interferometry of fully unsteady convection phenomena has been taken up as topic for future research.

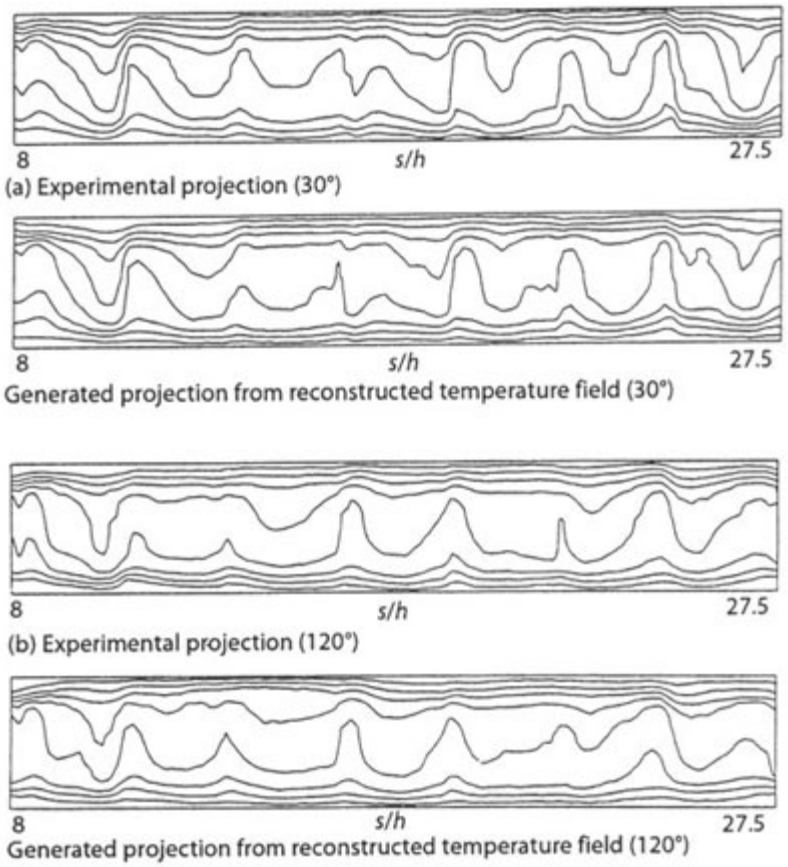

Figure 4.52: Comparision of experimentally obtained thinned images with generated projections for cross-checks of reconstructed temperature field, (a)Ra = 13900, 30°projection, (b)Ra = 13900, 120°Projection

Previous Next

Convection at Ra=1.39x10^4

The experiments at a Rayleigh number of 1.39 x 10^4 are considered first. Isotherms in the projection data at this Rayleigh number (Figure 4.53) in the 0° and 90° projections indicate the formation of longitudinal rolls in the fluid layer. For a cavity square in plan, the orientation of the rolls is indeterminate in principal, and will depend on mild imperfections in the experimental apparatus and non-uniformities in the thermal boundary condition. In the present work, the roll axis is seen to be parallel 90° to the view angle. The rolls are stacked adjacent to one another, but the roll-width is not a constant. Despite the presence of a dominant flow pattern, the temperature field is fully three-dimensional, as can be seen from the lack of straightness of the isotherms in the 0° projection. At the onset of longitudinal rolls in the fluid layer, scale analysis suggests the formation of as many rolls as the aspect ratio, 25 in the present experiment. The number of rolls seen in the projection data, Figure 4.39, is 15. The duration in the number of rolls with increase in Rayleigh number finds support in the work of Kolonder et al. [124]. These authors have reported a decrease in the number of rolls from 10 to 6 in a 10:5:1 cavity for a Rayleigh number increasing up to 2 x 10^4.

The loss-of-roll phenomena has been predicted using stability theory and summarized in Figure 2 of Busse and Clever [118]. This figure indicates that the movement of the flow state occurs along the stability boundary that separates skewed varicose (SV) instability form the knot (KN) instability in a direction of diminishing wave- number. In the present set of experiments, the Rayleigh number was increased form zero to its final value is one step rather than in a gradual sequence. Hence the transitions that would occur for a gradual change in Rayleigh number were not visible in the fluid layer. Thus the appearance of 15 rolls (instead of 25, as should happen if equal-sized square rolls were to be formed) at Ra=1.39x10^4 has been presented here, not as a transition point, but as a descriptor of the flow field.

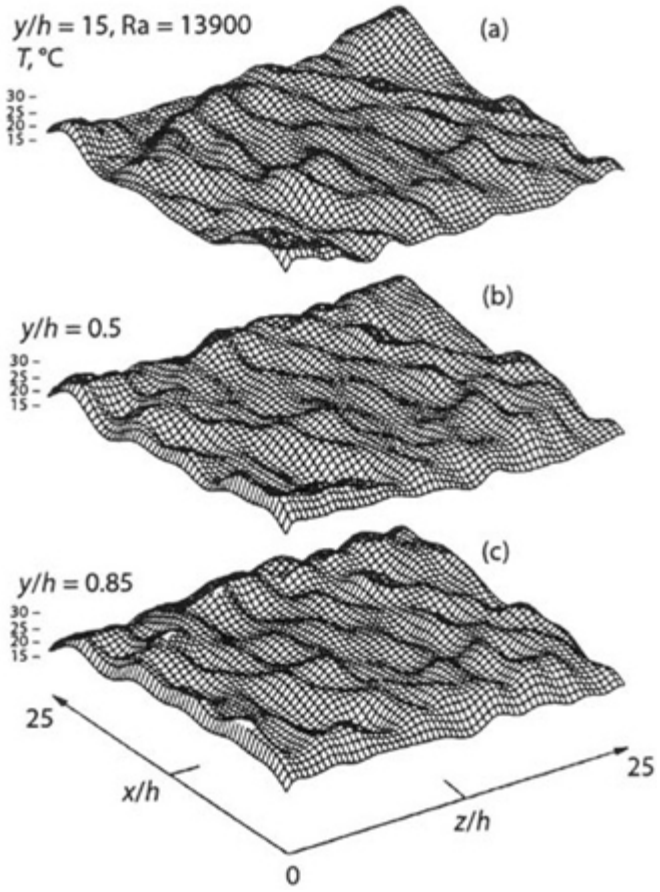

Figure 4.53: Temperature surfaces in the cavity at three horizontal planes, Ra-1.39x10^4, $(a)\, y/h = 0.15, (b)\, y/h = 0.5, (c)\, y/h = 0.85$

more...

Previous Next

Closure

A three-dimensional temperature field in a differentially heated horizontal fluid layer has been reconstructed from its interferometric projections. Two different Rayleigh numbers namely 1.39×10^4 and 4.02×10^4 have been considered. The tomographic reconstruction technique that has been employed AVMART. The algorithm converged without ambiguity to the final solution and did not display excessive sensitivity to the initial guess, relaxation factor, and noise in experimental data. The reconstructed field was seen to be fully consistent with the projection data. The reconstructed field was also seen to be in good agreement with the projection recorded, but not used in the tomographic algorithm. The three-dimensional field was seen to satisfy energy balance checks. the cavity-averaged Nusselt number computed from the interferometric projections was seen to be in reasonable agreement with published correlations.

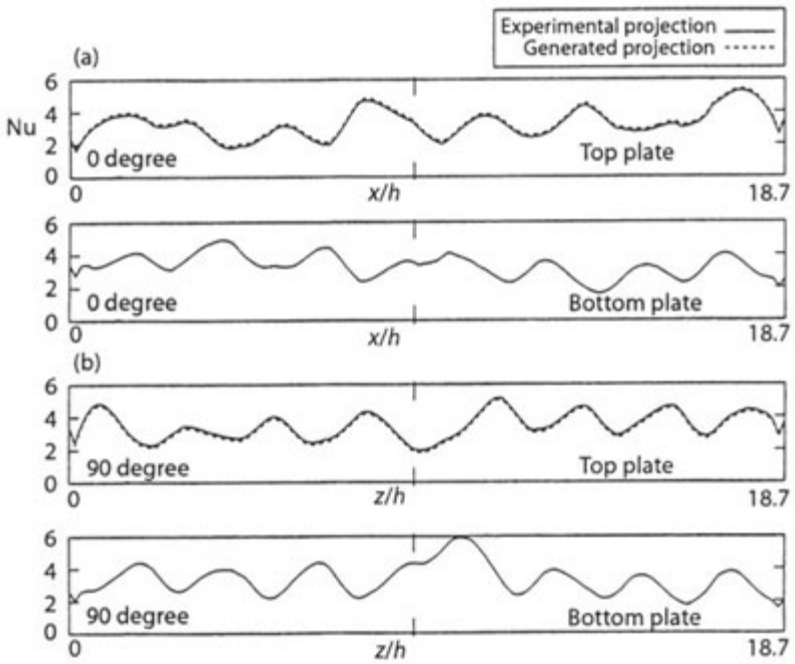

Figure 4.61: Comparision of experimentally obtained line-integrals of Nusselt numbers with generated line-integrals of Nusselt numbers, Ra=4.02×10^4, (a) 0° (b) 90° projections.

At a Rayleigh number of 1.39×10^4, the fringes were seen to be steady near the bounding walls, but mild unsteadiness was observed in the central horizontal players. At the higher Rayleigh number of 4.02×10^4, the unsteadiness was more pronounced, with flow switching between two well-defined states. The interfergrams corresponding to the dominant mode have been recorded and analyzed in the present work.

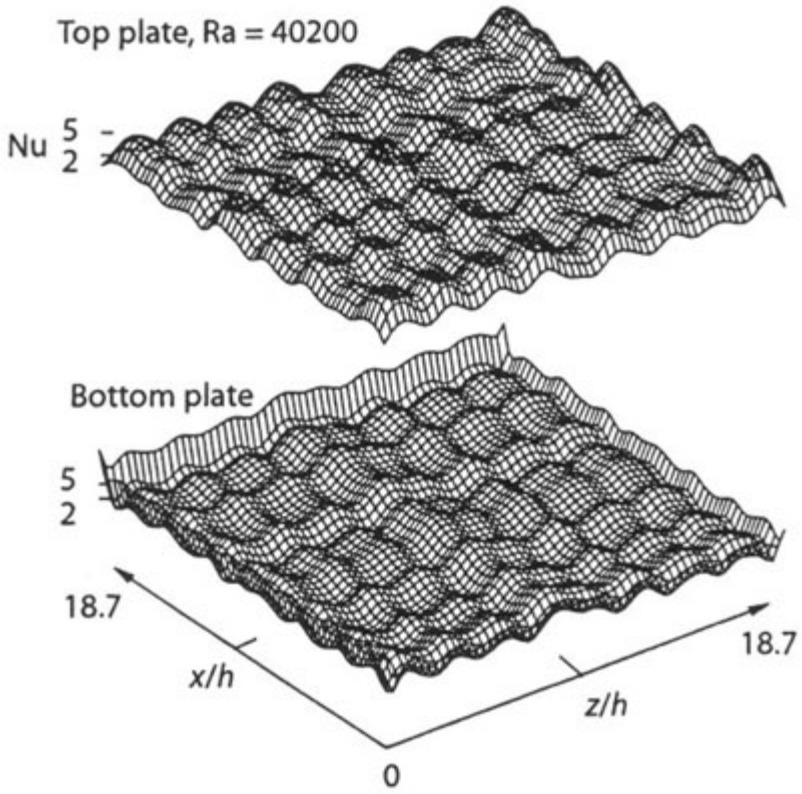

Figure 4.62: Nusselt number surfaces for top and bottom walls, Ra=4.02 x 10^4

At a Rayleigh number of 1.39x10^4 the flow field was seen to be organized in the form of a three-dimensional structure. A two-view tomographic calculation showed a set of longitudinal rolls as dominant pattern in the fluid layer. The rolls could be indentified from the projection data. The numbers of rolls was smaller than that based on the aspect ration consideration. The rolls also displayed three-dimensionality along its axis. At a Rayleigh number of 4.02 x 10^4, the thermal field was determined by cube-like ells that were spread all over the cavity. A collection of four cubic-cells was found to reveal a centrally located buoyancy-driven thermal plume rising from the hot plate and descending around it from the cold wall. The variation of the line-of sight averaged Nusselt number as a function of a wall coordinate at each of the hot and cold surfaces was seen to be consistent with the proposed flow models.

Previous Next

Figure 4.48 shows a collection of original interferograms at a Rayleigh number of 1.39×10^4 for a view angle of 90°. The roll formation, specifically five complete and two partial rolls are clearly seen here. For the cavity size studied, the number of rolls is in the range of 14-16. For compactness, thinned interferograms alone have been presented in this work. Figure 4.49 shows isotherms within the cavity for four different view angles at $Ra=1.39 \times 10^4$. As discussed earlier, the isotherms completely correspond to the fringe skeleton of the 0° and 90° projections. At other view angles, the corrospondence between fringes and isotherms is lost owing to changes in the path length traversed within the fluid layer, this is not a source of error since the geometric factor can be analytically accounted for. In the present work, the fringes have been mapped to temperatures over a grid and isotherms extracted from this data. Thus, thinned images for other view angles in figure 4.49 shows isotherms, determined from the interpolated grid values. Figure 4.40 shows thinned images of the fluid layer for a Rayleigh number of 4.02×10^4 at view angles of 0° and 90°.

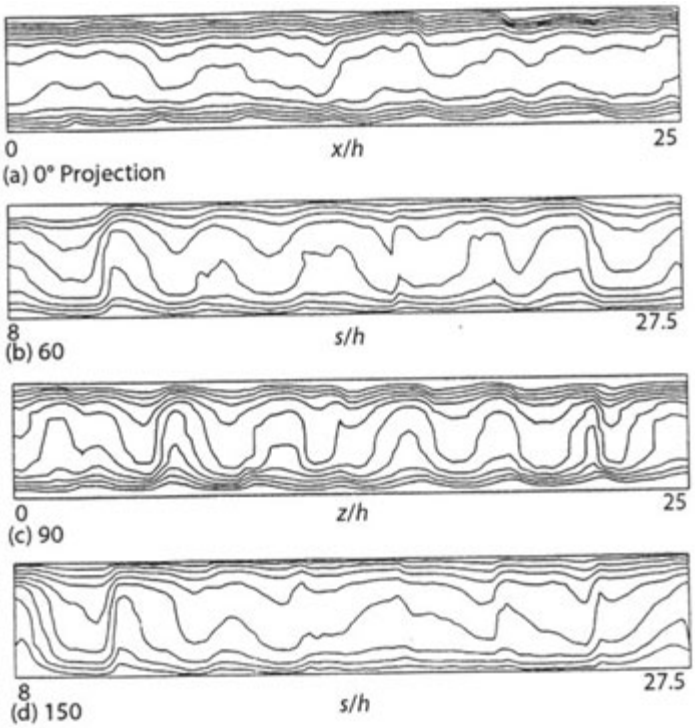

Figure 4.48: Thinned images of the cavity $Ra=1.39 \times 10^4$, $(a)\ 0^\circ\ (b)\ 60^\circ\ (c)\ 90^\circ\ (d) 150^\circ$ projections.

The correctness of fringe thinning, assigning fringe temperatures, and a check on the magnitude of interpolation errors have been examined by using the following result: at steady state, the width-average of the line integrals of temperature field ploted as a function of the vertical coordinate is independent of the projection angle. This is because the total energy transferred across the cavity is unchanged from one horizontal plane to the next.

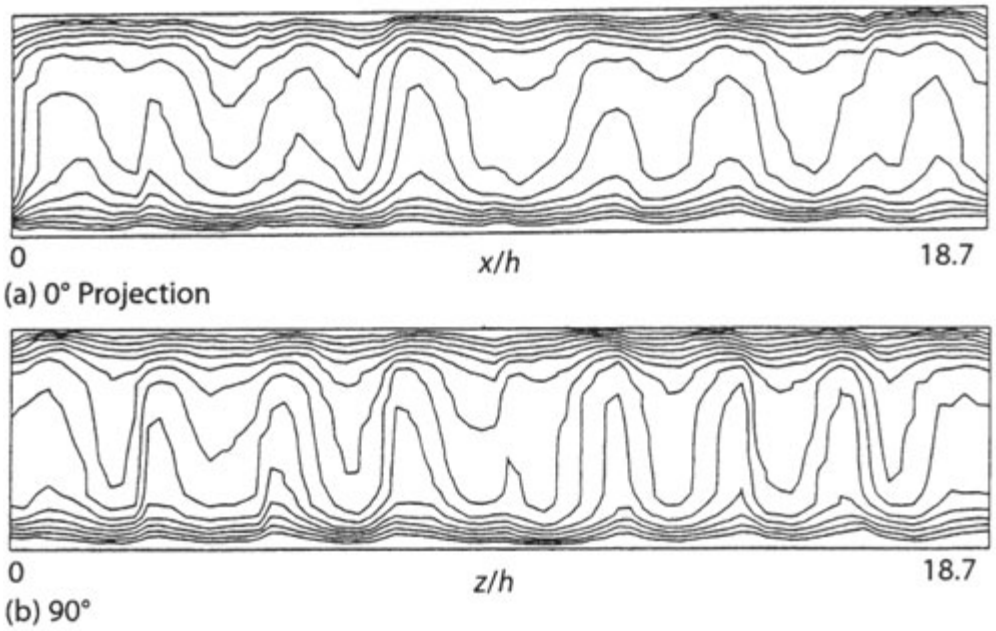

Figure 4.49: Thineed image of the cavity, Ra=4.02 x 10^4, (a) 0˚, (b) 90˚

Previous Next

Figure 4.50 shows the variation of line integrals of the temperature field averaged over a horizontal plane as function of the vertical coordinate measured form the cooled top wall for both 0° and 90° projections at Rayleigh number of 1.39×10^4. The corresponding graph for Ra=4.02 x 10^4 is shown in Figure 4.51. The S-shaped curve, characteristic of buoyancy-driven convection can be seen here. The curves for the two projections match closely and their slopes at the hot and cold walls are practically equal. The S-shaped curve for the angular projection have not been shown since the corresponding projection data have been subsequently corrected to ensure that between the two projections, the S-shaped curve is strictly unique. This step did not alter the isotherms in Figures 4.50 and 4.51 to any significant degree, but was expected to improve convergence of the tomographic inversion process.

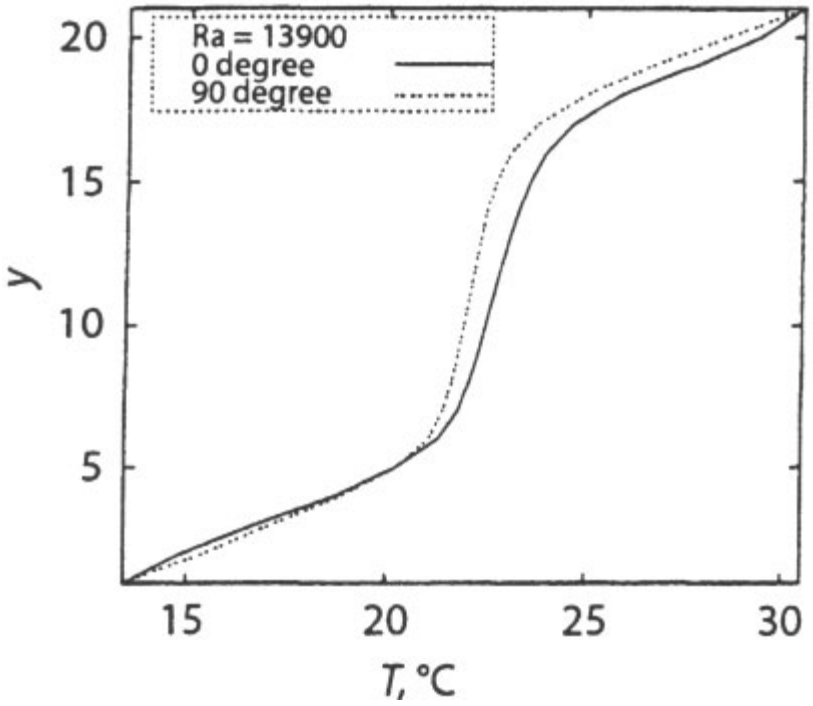

Figure 4.50: Width averaged temperature profile in the cavity, Ra=1.39×10^4 (y=1 is the top wall.)

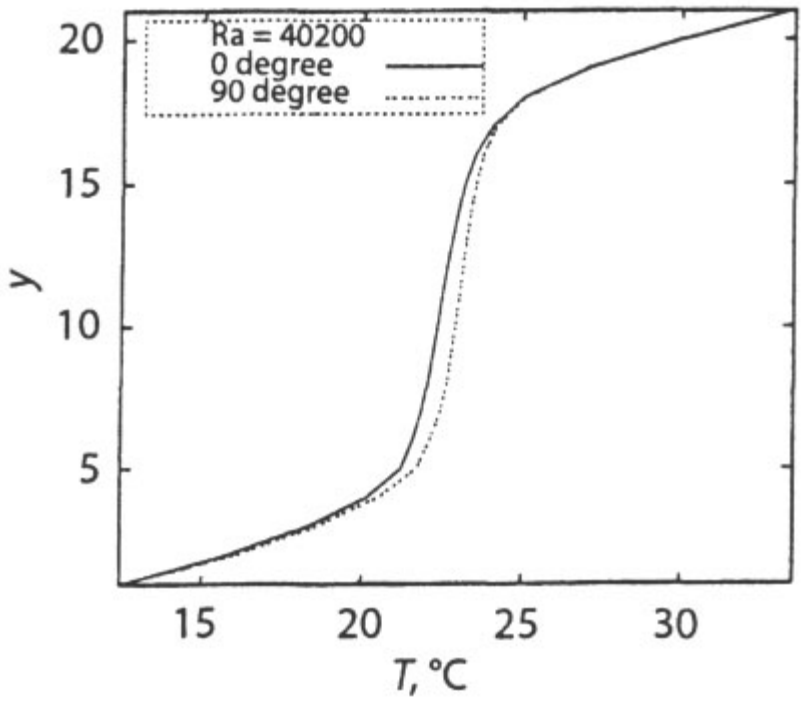

Figure 4.51: Width averaged temerature profiel in the cavity, Ra=4.02 x 10^4 (y=1 is is the top wall.)

Previous

For 25 rolls, the dimensionless wave number $\gamma \; is \; \pi$ is while it decreases to 1.88 for 15 rolls. This places the flow regime in a state of oscillatory instability [118]. The mild unsteadiness in the fringe patterns can be with the oscillatory instability mechanism corresponding to a Rayleigh number 1.39 x 10^4 and a dimensionless wavenumber of 1.88.

The temperature surfaces on three horizontal planes at which $y/h = 0.15, 0.5, and 0.85$ respectively, are shown in Figure 4.53. To preserve visual clarity, these surface plots have been partially filtered, without any noticeable loss of signal strength. The ordering of the horizontal planes is from the cooled top plate where $y = 1$. The nature of the temperature field is three-dimensional but is similar at all the three planes. One can see rolls spreading over the entire length of the cavity. While this is a qualitative trend, distortions can also be seen in the form of nonuniformity in roll width and straightness, and possible interference between neighboring rolls. These aspects are brought out in the isotherms over horizontal planes of the fluid layer (Figure 4.54(a-c)) as the equivalent or the dominant rend, with other detail surfacing from increasing view angle. The patterns on two different planes obtained with the final set of four views $(0^\circ, 60^\circ, 90^\circ, and \; 150^\circ)$ are shown in Figures 4.54 (b-c). These figures have also been partially filtered for presentation. While the unfiltered plots satisfy the projection data, the isotherms in Figure 4.54 are quite close. Hence, the resulting influences of the apparently three-dimensional flow field Figure 45 (b-c) is akin to longitudinal rolls. While Figure 4.54(b-c) show three-dimensionality in the flow field, the similarity in the geometry of isotherms suggests the formation of a stable structure in the field layer. The situation is analogous to chaotic convection superimposed on a set of stationary rolls observed by Gollub and Benson at a Rayleigh number of 60000.

The local, the line-of-sight averaged (i.e., along a light ray) and the cavity averaged Nusselt numbers have been computed at both the walls. The Nusselt number has been computed using the reconstructed filed as well as the projection data. The average Nusselt number for the entire surface has been computed form the width-averaged temperature profile of the projection data. This corresponds to the slope of the S- shaped curve at the bounding planes. The average Nusslet number at both plates has been reported for various angles of projection. The angular projections other than Ra=4.02 x 10^4 do not include the entire width of the test cell, but it is expected that the average Nusselt number over the partial length will be representative of the entire width of the cavity. The average Nussselt number for each of the plates has been compared with the experimental correlation reported by Gebhart et al. in air.

A summary of all the Nusselt numbers referred to above is given in Table 10. The Nusselt numbers computed form interferometric measurements are within $\pm 10\%$ of the globally averaged value of 2.14. the individual plate-averaged Nusselt numbers are 2.16 and 2.12 as shown within brackets in Table 10. As stated earlier, interferometric projections at $30^\circ and 120^\circ$ were not utilized for reconstruction. The closeness of the average Nusselt numbers at these view angles with respect to other projections shows overall consistency in the measurements. The above equation gives a value of Nu=2.59 at Ra=1.39x10^4. The Nusselt number obtained form the present set of experiments is thus approximately 17% below the Nusselt number based on the above correlation. The agreement is much closer at the higher Rayleigh number and is discussed later. Within experimental uncertainty, the comparison with previous experiments at the lower Rayleigh number may be taken to be favorable.

Table 10: Comparision of Average Nusselt Number with Ra=1.39x10^4

Projection angle in degree	Nu (cold Surface)	Nu (hot surface)	Nu (average) From all angles	Nu (reference)
0	2.18	1.94	2.12 (hot)	2.59
30	2.33	2.02	2.16 (cold)	
60	1.99	2.34	2.14 (cavity)	
90	2.00	2.17		
120	2.19	2.32		
150	2.27	1.95		

The temperature field derived form the interferograms suggest the formation of longitudinal rolls in the cavity. The presence of rolls can be deduced form local Nusselt number variation the distance. When the local Nusselt number is computed from the projection data, the value corresponding to the average computed along the light ray within the test cell is obtained. These line-of-sight Nusselt numbers are averaged along the direction of the light ray and are shown in Figure 46 for various projections angles for the top and the bottom plates. The rolls being parallel to the axis, the line-averaged Nusselt number along the axis that is the projection is expected to show similar trends over both the walls. This is evident in Figure 4.54 (a), where except for a small part of the test cell towards the ends, the local hot and cold wall Nusselt numbers are similar. Along the axis, that is the projection, the local Nusselt numbers at the two walls are expected to show a phase shift. This corresponds to the inclination of the major axis of the roll cross-section with respect to the vertical direction. This shift is seen in Figure 4.54 (b). Hence in a qualitative sense the variation of the line-averaged Nusselt number over the two plates supports the equivalent flow pattern in the cavity to be in the form of longitudinal rolls.

Previous Next

contd...

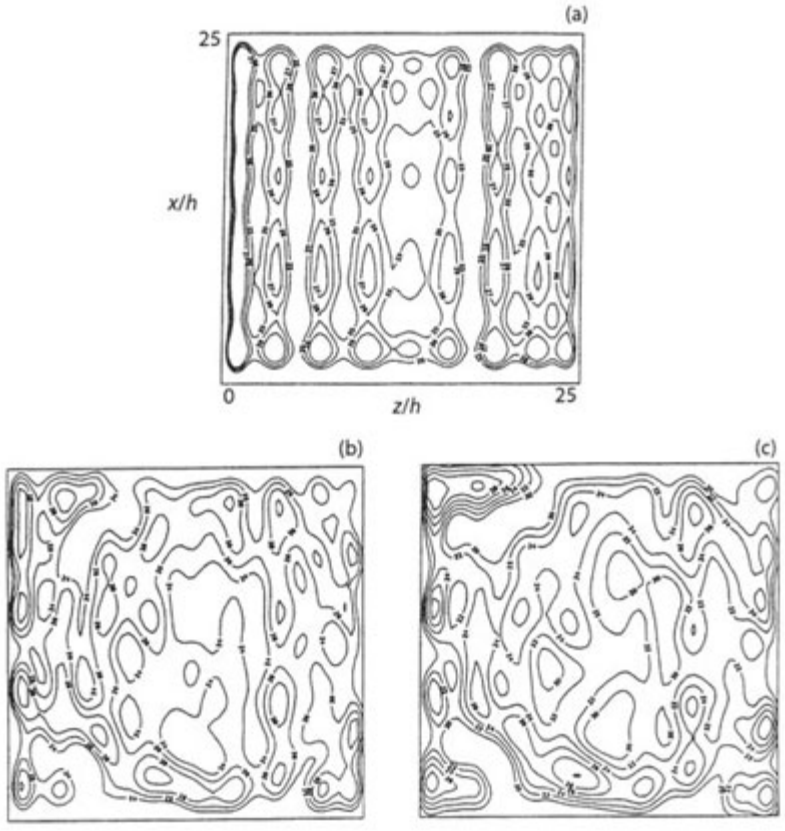

Figure 4.54: Isotherms on horizontal planes of the fluid layer, Ra=1.39x10^4. $(a) y/h = 0.15, (b) y/h = 0.5, (c)\ y/h = 0.85$

The local Nusselt number along the direction of the projection angle shows definite variations with distance. This suggests three-dimensionality in the longitudinal rolls which are no longer two-dimensional at the Rayleigh number studied. The loss of two dimensional structure in the rolls can also be confirmed from other projections (Figure 4.55 (c) - 4.55(f)). Since the rolls identified in the projection data are parallel to the axis, projections symmetric with respect to the axis will be identical at the limit of strict two-dimensionality. A comparison of projections obtained from summetrically placed angles, namely (30, 150) and (60, 120) shows qualitative similarity. This strengthens the suggestion of rolls, but also highlights their unequal sizes and their three-dimensional nature along the roll axis.

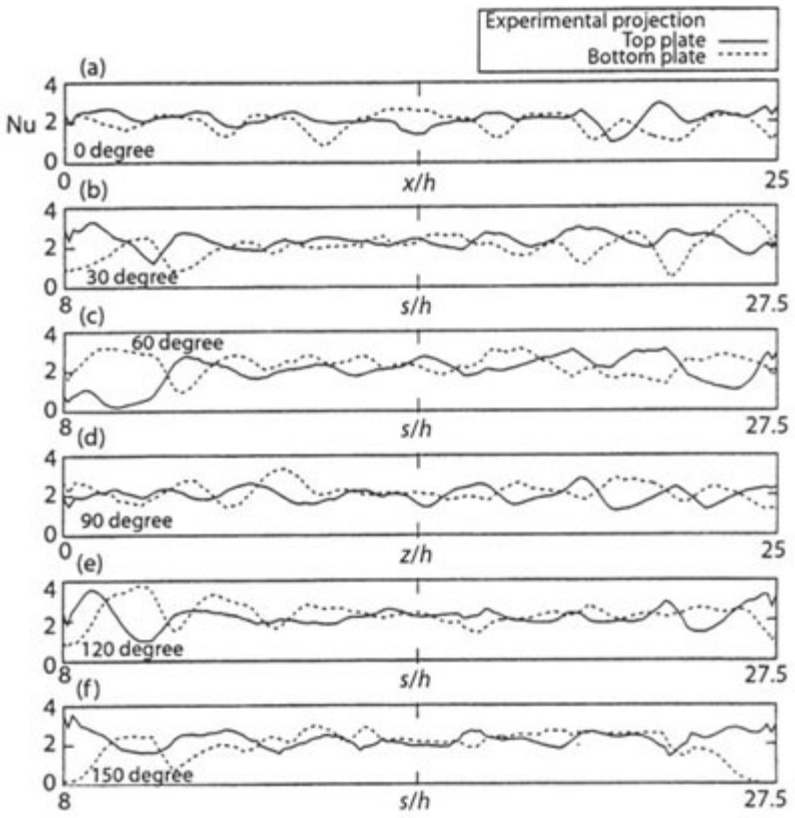

Figure 4.55: Experimentally obtained line-integrals of Nusselt numbers for both the walls, Ra = 13900, (a) 0°, (b) 60°, (c) 90°, (d) 90° (e) 120° (f) 150° projections

The Nusselt surface obtained from the reconstructed temperature field is shown for each of the hot and cold surfaces in Figure 4.56. Along the rolls axis, the Nusselt number surfaces of the top and bottom plates are oppositely oriented. Heat transfer form the lower to the top plate by a buoyancy-driven roll is associated with the peaks and valleys of the Nusselt number surface.

Previous Next

Convection at Ra=4.02 x 10^4

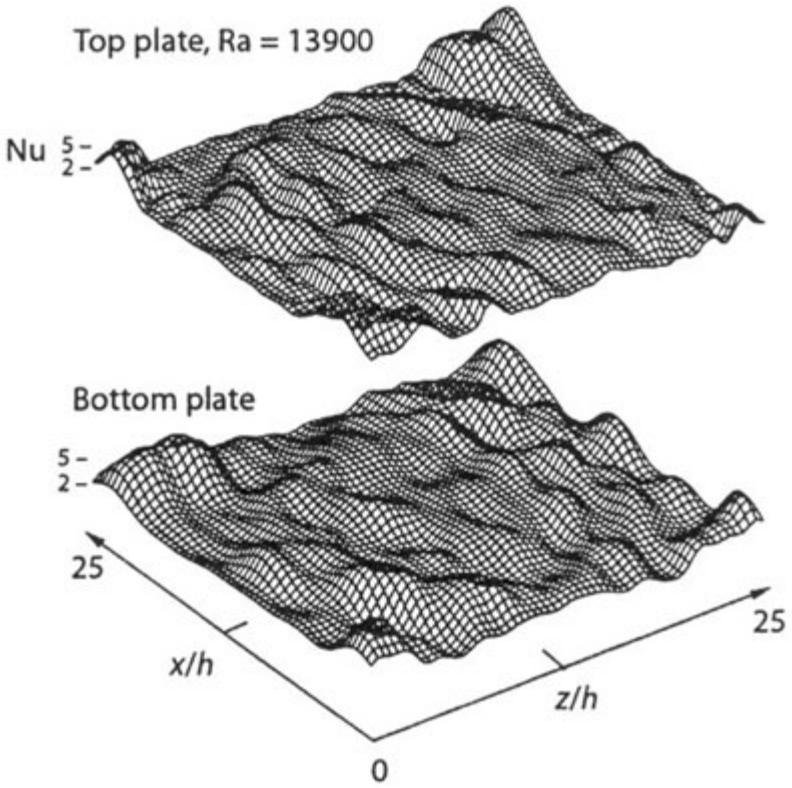

Figure 4.56: Nusselt number surfaces for top and bottom walls, Ra=1.39x10^4

Analysis of results from the experiments at a Rayleigh number of 4.02 x 10^4 are presented next. In the higher Rayleigh number experiment, formation of a hot buoyant plume arising from the bottom plate and advancing towards the cold top plate has been observed. Since the discussion is based on two views, structures referred to below are to be interpreted are representative of the flow field. The temperature surfaces, namely the temperature variation over horizontal planes, are shown in Figure 4.57. Three horizontal planes, namely $y/h = 0.15, 0.5, \text{and} 0.85$, have been considered. A clearer picture emerges when isotherms at the corresponding planes over an assembly of four adjacent cells are examined. This is shown in Figure 4.58. Here, each cell corresponds to the portion of the cavity reconstructed from the interferograms. On assembly, the collection of temperature surfaces over the three planes clearly shows the structure of a rising plume. The repeating roll-like structure seen the from the both the $0^\circ \text{and} 90^\circ$ view angles suggests that a cubic cell exists inside the cavity. Mukutmoni and Yang [102] have shown the formation of an oscillatory polygonal planform structure for intermediate aspect ration boxes for a fluid of Prandtl number equal to 3.5 at a Rayleigh number of 2400. The present observation that flow organizes in the form of cubic cells in the cavity is similar to their conclusion. It is also in agreement with the authors' previous study based on partial projection data with two view angles [79].

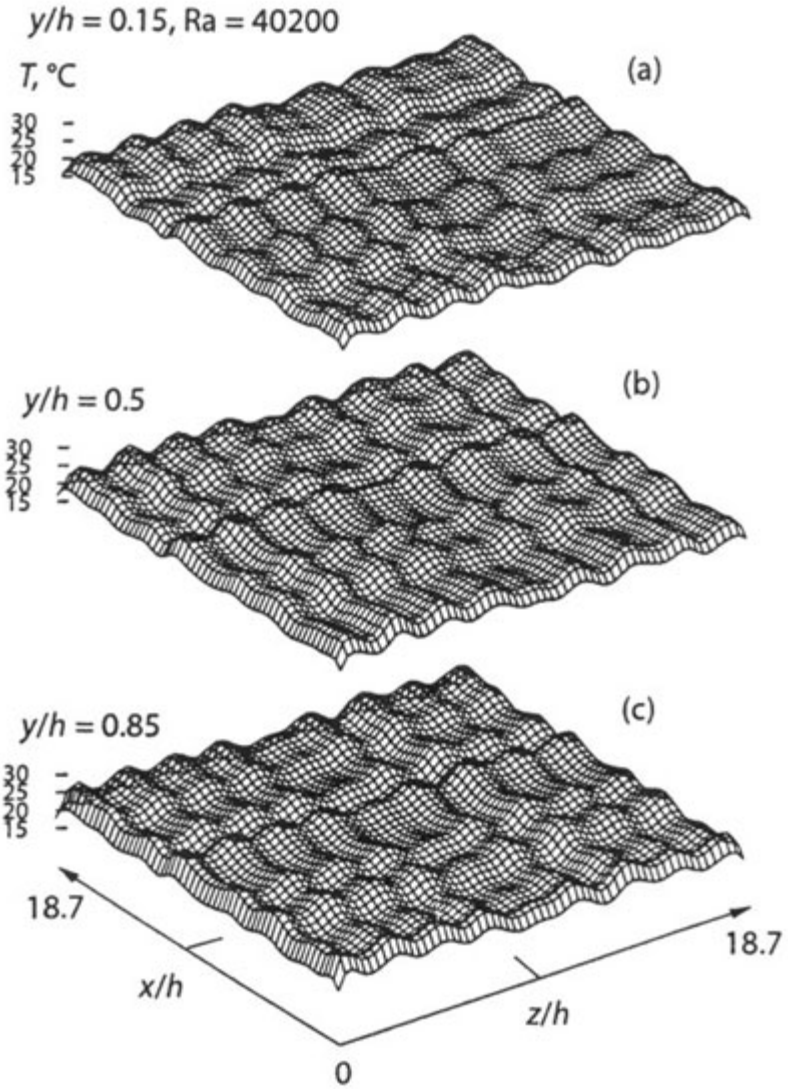

Figure 4.57: Temperature surface in the cavity at three horizontal planes, $Ra=4.02x10^4$

Figure 4.58 shows that the size of the heated region increases as one moves towards the heated lower wall. The buoyant plume rises from the center of the cluster of four adjacent repeated cubic cells. Each cubic cell can be visualized as being divided along its diagonal plane with high- and low-bulk-fluid temperatures on each side. Thus, the fluid rising along the center descents uniformly around the plume in the four quadrants. The assembly of four cells encloses a set of four rolls, all of which raise hot fluid jointly along the central vertical axis, which after being cooled, descents all around towards the lower surface. While it is possible to identify a cubic cell that is isolated from a thermal viewpoint (for example from the interferograms), it should be noted that the associated velocity field need not be isolated. In fact, the velocity field in individual cubic cells will interact and an orderly pattern for flow can be discerned only over a collection of cells.

Previous Next

A flow model that integrates all aspects of the temperature contours is shown in a schematic diagram in Figure 4.59. This Figure shows the hot mass of fluid rising in the form of a buoyant fountain form the center of the four adjacent cells and distributing the cold fluid in the four quadrants from above, almost symmetrically. When viewed from any direction this flow field will show a roll-like repeating structure. The plume cross-section is not seen to be of any definite shape, but is closer to an ellipse than a circle. This is simply because the cubic cell has unequal edges.

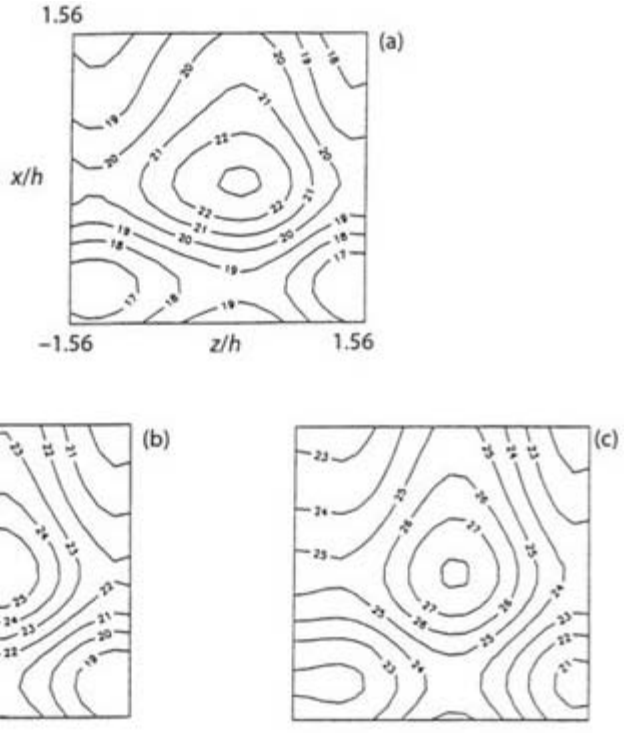

Figure 4.58: Isotherm in the cavity at three horizontal planes, Ra=4.02 x 10^4, $(a)\, y/h = 0.15, (b)\, y/h = 0.5, (c)\, y/h = 0.85$

At a Rayleigh number 4.02 x 10^4, the average dimensionless wave-number of the dominant roll-pattern was found to be 2.52. The stability diagram of Busse and Clever [118] does not extend beyond Ra = 2 x 10^4. However, an examination of the stability diagram for Pr=7 (water) is possible though it is known that a higher Prandtl number has a stabilizing effect. The point $\mathrm{Ra} = 40200 \text{ and } \gamma = 2.52$ falls very close to the cross-roll stability boundary. The corresponding shadowgraph images are vividly shown by Busse and Clever [118], and Nasuno et al. [117].

The work of Busse and Clever [118] shows that the approach to cross-rolls in water is via skewed varicose and knot instabilities as the Rayleigh number is raised. In contrast, at Pr =0.7 the sequence is skewed varicose, oscillatory, and with knot instabilities, but no data is really available for Ra> 15000. As discussed below, Lipps [127] has shown the formation of (semi) cross-rolls at Ra =2.5 x 10^4 in a small aspect ratio fluid layer. The formation of cubic cells as dominant pattern, and a switch between this pattern and longitudinal rolls have been observed at Ra =4.02 x 10^4 in the present experiments. This suggests that the boundaries of the oscillatory, knot, and cross-roll regimes (when extended) should be in the vicinity of this Rayleigh number in air. As in the case with Ra =1.39x10^4, one cannot comment on the route followed in the present experiments by the flow field to attain its

final state on the stability diagram.

Previous Next

The analysis of the temperatures field reported in the present study is based on the dominant fringe patterns. It was not possible to capture the momentary appearance of the secondary mode, but a visual examination showed it to be straight fringes, and hence equivalent to a longitudinal roll. The estimated to be around ten seconds, corresponding to a frequency of 0.1Hz and a Fourier number $(\alpha t/h^2)$ of 0.25. Frequencies of a similar order of magnitude have been reported by Gollub and Benson [126] in their LDV study of RB convection at Rayleigh numbers up to 100 times the critical Rayleigh number for the onset of convection.

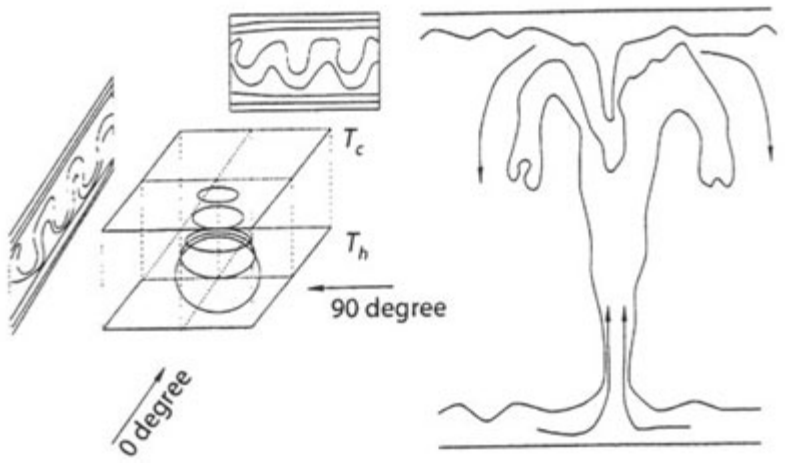

Figure 4.59: Schematic of the cubic cells and rising plume inside the cavity

The experimental results are compared next with those of Lipps [127]. This is a numerical study of Rayleigh-Benard convection in air over the range 4000<Ra <25000. The comparison is between the present experiments at Ra=4.02 x 10^4 (aspect ratio= 1800) and the numerical prediction at Ra=25000 (aspect ratio = 5-6). Thos the comparison is at best qualitative. Lipps [127] has reported time-dependent oscillation in the fluid layer whose characteristic time scales are position dependent. On the midplane of the fluid layer, this was in the range $0.05 < \tau < 0.2$. The mean flow itself had a periodicity of $\tau \approx 1.3$. The corresponding number for the present experiments based on visual judgment was 0.25, as mentioned in the previous paragraph. Despite this difference, typical isotherms shown by Lipps [127] are remarkably similar to the interferograms recorded in the experiments. Numerical calculations do not reveal plume formation, and instead, the author has indentified a tongue-like structure spreading in the horizontal plane.

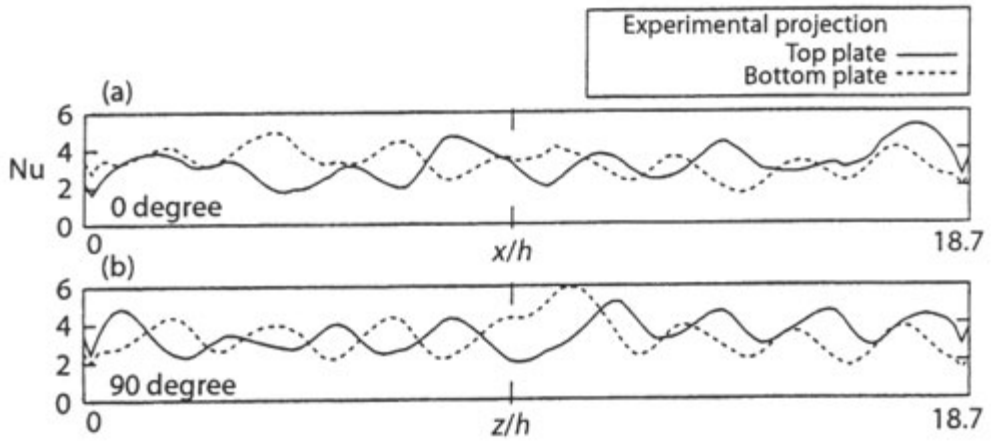

Figure 4.60: Experimentally obtained line-integrals of Nusselt numbers for both the Walls, Ra=4.02 x 10^4, (a) 0° (b) 90°

Previous Next

Lipps [127] has reported the appearance of a dominant flow pattern in the shape of a (semi) cross-roll followed by a disturbed flow regime, and the time scale for the switch-over was $\tau \approx 1.3$. This result has a definite similarity with the experiments of the present study, in which the switching phenomenon has been reported. The time scale seen in the experiments (=0.25) is similar than1.3, but can be explained as being due to

- A higher Rayleigh number which tends to lower the time scales, and
- A higher aspect ratio which can active a whole range of wave numbers including small ones thus causing a lowering of τ

Results for the Nusselt number at a Rayleigh number of 4.02 x 10^4 are presented next. The numbers averaged over the entire surface are given in Table 11. These have been compared with the correlation of Gebhart et al. [89]. The agreement between the Nusselt numbers of the present work and the correlation can be seen to be close. Specifically, the Nusselt number computed from the present set of experiments is within 1.5% of the empirical correlation.

The variatrion of the line-of-sight averaged Nusselt number with distance closely reflects the flow pattern in the cavity. As in the case of tge lower Rayleigh number, these have been computed directly from the interferograms and are shown in Figure 4.60.Both 0° and 90° projections have been presented. A roll-like structure can be seen from both view angles and so the Nusselt number variation is expected to be oppositely oriented for the two active surfaces. This result is clearly brought out in Figure 4.60. The line-of-sight averaged Nusselt numbers were also compute from the reconstructed (fully three-dimensional) temperature field. The comparison between the reconstructed and the original local Nusselt numbers is presented in Figure 4.61. For the and view angles that have been employed in reconstruction, the comparison for both surfaces is excellent. The Nusselt number surfaces over the two bounding planes are shown in Figure 4.62. These surfaces are clearly oppositely oriented at the hot and cold walls. This confirms that when visualized from any angle, the resulting fringe pattern will be a roll-like repeating structure. It strengthens the suggestion made that the flow field is in the form of a buoyant plume.

Table 11: Comparision of Average Nusslt number with [89], Ra=4.02 x 10^4

Projection angle in degree	Nu (cold surface)	Nu (Hot surface)	Nu (average) from all angles	Nu (reference)
0	3.22	3.30	3.32	3.28
90	3.48	3.30		

Previous